Article:
Ahmad, R, Cochrane, RF and Mullis, AM (2012) The formation of regular alpha Ni- gamma (Ni31Si12) eutectic structures from undercooled Ni-25 at.% Si melts. Intermetallics, 22. 55 - 61 . ISSN 0966-9795

https://doi.org/10.1016/j.intermet.2011.10.021

The Formation of Regular αNi-γ($Ni_{31}Si_{12}$) Eutectic Structures from Undercooled Ni-25 at.% Si Melts.

R. Ahmad[†]*, R.F. Cochrane & A.M. Mullis*[‡]

Institute for Materials Research, University of Leeds, Leeds LS2-9JT, UK.

Abstract

Undercooling experiments have been performed on an Ni-25.2 at.% Si alloy using a flux encasement technique, with a maximum undercooling of 160 K having been achieved. Double recalescence was observed at all undercoolings, with crystal growth velocities being measured for the first recalescence event. These velocities were extremely low, with a maximum value of 0.018 m s^{-1} being recorded. At all undercoolings a eutectic structure was observed, comprising alternating lamellae of single phase γ($Ni_{31}Si_{12}$) and Ni-rich lamellae containing of a fine (200-400 nm) dispersion of βNi_3Si and αNi. This is contrary to the equilibrium phase diagram from which direct solidification to βNi_3Si would be expected for undercoolings in excess of 53 K. We postulate that the direct solidification of βNi_3Si from the melt is suppressed, with an α-γ eutectic being formed instead. The α appears to be supersaturated in Si and undergoes a eutectoid decomposition to α and βNi_3Si, giving rise to the observed second recalescence.

Keywords: C. rapid solidification processing; A. silicides, various; D. microstructure.

1. Introduction

Practical interest in intermetallics centres on their potential utilisation as high temperature structural materials due to their high hardness and good chemical stability at elevated temperature. One such is βNi_3Si, which displays excellent high temperature oxidation resistance, is generally resistant to corrosion in acid environments and has a yield strength which increases with temperature [1]. However, like many other intermetallics, a major obstacle to the greater utilisation of βNi_3Si is its lack of room temperature ductility, which inhibits formability. One potential route to mitigate against this limitation is to incorporate a ductile phase into the brittle intermetallic matrix and for this reason [2] considerable interest has been focussed on the Ni-rich end of the Ni-Si system, wherein an eutectic between αNi and βNi_3Si can be formed.

Another potential route to mitigate against the limitations imposed by the poor room temperature ductility of intermetallics is non-equilibrium processing [3], such as by rapid solidification. There have been several such studies on the Ni-Si system, mostly concentrated on the eutectic composition, Ni-21.4 at.% Si. The focus of this research has been mainly on microstructural evolution within the eutectic, together with phase selection and metastable phase formation. One of the first such studies was by Wei

[†] Now at Mechanical Engineering Department, Faculty of Engineering, University Malaya, 50603 Kuala Lumpur, Malaysia.

[‡] Corresponding author.

and Herlach [4], who observed a gradual transition from lamellar to anomalous eutectic microstructure as the undercooling was increased, with the onset of the anomalous eutectic structure being observed at an undercooling of $\Delta T = 31$ K. The transition to the fully anomalous structure was complete at $\Delta T \sim 150$ K, with only the αNi and βNi_3Si phases being present. Later work by Leonhardt *et al*. [5], managed to achieve an increased undercooling level of 250K, wherein a double recalesence event could be observed. Moreover, by quenching the undercooled sample onto a chilled substrate the formation of metastable $Ni_{25}Si_9$ was observed. The highest undercooling to be reported for this material was 550K by Lu *et al*. [6] and Liu *et al*. [7], using a combination of the melt fluxing and cyclic superheating techniques. With increasing undercooling the as-solidified microstructure displayed a complex evolutionary sequence from regular lamellar eutectic, via irregular lamellar eutectic, coarse directional dendritic, quasi-spherical eutectic colonies, and fine directional dendritic to anomalous eutectic. They also observed a significant refinement of the grain structure with increased undercooling, which they attributed to enhanced nucleation, although many other mechanisms have been suggested to account for grain refinement in deeply undercooled melts, including post-recalescence remelting [8] and the development of growth instabilities [9, 10].

Recently Lu *et al*. [11] have extended their analysis to include Ni-29.8 at.% Si eutectic alloy, observing what they described as an interlaced morphology. This they attributed to the initial formation of γ ($Ni_{31}Si_{12}$) which subsequently remelted during recalescence to be replaced by an ordered δ-phase (Ni_2Si). At undercoolings in excess of 340 K [12] the microstructure showed a transition from a regular to a quasi-regular structure, which was attributed to the evolution from a faceted/faceted eutectic to a non-faceted/non-faceted eutectic (possibly with a faceted/non-faceted intermediate state). Intriguingly, Lu *et al*. [13] also observed that when an undercooling in excess of 240 K was combined with a cooling rate of > 1 K s^{-1}, small amounts of an amorphous phase were formed. If correct, this constitutes an exceptionally low cooling rate for amorphous phase formation in a binary alloy.

However, the direct rapid solidification of the intermetallic, without the formation of a second ductile phase, is also a recognised [14] way to improve the mechanical properties. Increased chemical disorder or the formation of antiphase domains improves the room temperature ductility thus making it less difficult to machine or forge the intermetallic to near net shape. In this paper we report upon undercooling experiments performed on Ni-Si melts at the nominal Ni_3Si composition.

The equilibrium phase diagram for the Ni-rich end of the Ni-Si system [15] is shown in Fig. 1. Ni_3Si occurs in both low (β_1) and high (β_2/β_3) temperature forms, with these having the $L1_2$ and $D0_{22}$ crystal structures respectively. In addition, the high temperature phase has both an ordered and disordered form (β_2 and β_3 respectively), giving rise to the three forms shown in the phase diagram. The temperature stability fields are $1388\ K \leq T \leq 1443$ K for β_3, $1263\ K \leq T \leq 1388$ K for β_2 and $T \leq 1308$ K for β_1. The two high temperature polymorphs have a compositional range of 25.0-26.1 at.% Si, while the low temperature β_1 form has a compositional range of 22.6-24.5 at.% Si. There is no overlap of these composition ranges, potentially complicating the analysis of the solidification of β-Ni_3Si from its undercooled parent melt should a wide range of undercoolings be employed.

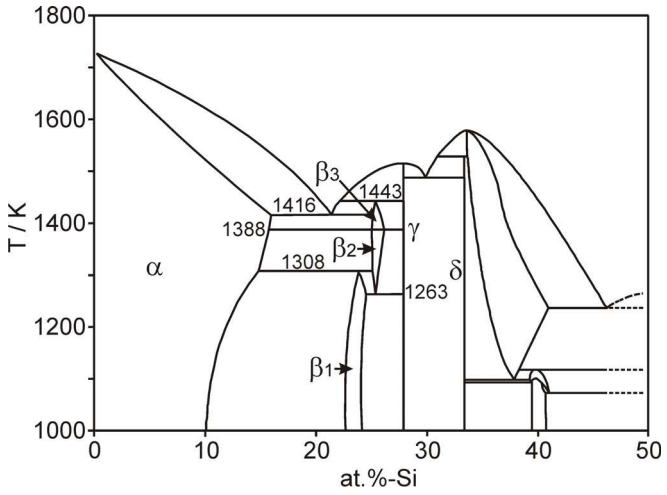

Figure 1. Ni-rich portion of the Ni-Si phase diagram, showing three variants of the βNi_3Si intermetallic. β_1 is a low temperature form with the $L1_2$ crystal structure, β_2 and β_3 are high temperature polymorphs with an ordered and dis-ordered DO_{22} crystal structure respectively.

The equilibrium solidification path from the melt for an alloy of initial composition around 25 at.% Si would be for the growth of γ-phase ($Ni_{31}Si_{12}$), with the subsequent conversion to β_3 via a peritectic reaction below 1443 K. Upon further cooling β_3 will transform polymorphically to β_2, before finally undergoing an eutectoid reaction to give $\beta_1 + \gamma$. However, for modest undercooling direct solidification to β should be available. The undercooling required for such direct access to the β-phase to become available can be estimated via the metastable extension of the β-liquidus line, which can be calculated using the CALPHAD method. This has been undertaken using the commercial software package MTDATA [16], wherein we find that at a composition of 25 at.% Si, the metastable liquidus is some 10 K above the peritectic temperature (1443 K). With the γ-liquidus at this composition estimated at 1496 K direct access to β should become possible at a minimum undercooling of 43 K.

The undercoolings required to directly access the β_2 and β_1 phases is more difficult to estimate due to the imperfect thermodynamic representations of these phases in the currently available SGTE solutions data base [17]. However, taking the equilibrium stability fields as a guide, we would estimate that β_2 would be accessible in the undercooling range $108\ \mathrm{K} \le \Delta T \le 233\ \mathrm{K}$ and β_1 for $\Delta T \ge 188\ \mathrm{K}$, although these figures should be taken as rough estimates only. Given the relatively high undercooling probably required to access the β_1 phase directly, it has been decided here to focus on a composition appropriate to the β_2/β_3 phase and, if necessary, restrict the range of undercoolings studied.

Undercooling and growth velocity studies have previously been undertaken on a number of closely related intermetallic systems including CoSi [18], γ-TiAl [19], Fe_3Ge [20] and Ni_3Ge [21]. Close to equilibrium CoSi grows as an ordered phase direct from the liquid but, as predicted by Assadi & Greer [22], with increasing undercooling disorder trapping will occur leading to a sharp rise in the growth velocity at the point where the growing solid becomes completely disordered. In the case of CoSi this transition occurs at an undercooling of 310 K, corresponding to a

critical growth velocity of ≈3.8 m s^{-1} [18]. Similar behaviour is seen in Ni_3Ge, with the critical undercooling for complete disordering being observed as 168 K, corresponding to a much lower critical growth velocity of ≈0.22 m s^{-1}. In γ-TiAl the ordered γ-phase gives way to the disordered phase above an undercooling of 150 K, wherein there is a discontinuous jump in the crystal growth velocity from 0.5 m s^{-1} to ~10 m s^{-1} [19]. For Fe_3Ge the transition to collision limited growth was not observed even at the highest undercooling obtained ($\Delta T = 160$ K) [20], with the maximum observed growth velocity being 1.3 m s^{-1}. For Ni_3Si, growth at high temperature ($1388 \text{ K} \leq T \leq 1443$ K), corresponding to the low undercooling regime $43 \text{ K} \leq \Delta T \leq 108$ K should result in the growth of the disordered β_3 phase, with direct access to the ordered phase only being available for high undercoolings, giving rise to the prospect of rather more complex behaviour.

2. Experimental Method

The target composition for the undercooling experiments was chosen as Ni-25.3 at.% Si, as this corresponds to the region of the phase diagram over which the β_2/β_3 phase has the greatest temperature stability range (see Fig. 1). The alloy was produced by weighing and mixing elemental Ni and Si of 99.999% purity (metals basis) which were then then formed into 10 mm pellets to be arc melted under an argon atmosphere. Arc melting of the pellets was repeated at least 10 times in order to ensure thorough mixing of the constituent elements. The pellets were weighed subsequent to arc melting to ensure no loss of material and were then re-melted into ingots ~ 60 mm long and 6 mm in diameter. These ingots were sealed, under an argon atmosphere, into silica tubes so that the material could be homogenised at 1250 K. Typical homogenisation times were around 200 hours. Following homogenisation, EDX analysis of the resultant ingots was undertaken to check the composition, which was measured at Ni-25.2 at.% Si.

Undercooling experiments were performed within a stainless steel vacuum chamber evacuated to a pressure of 5 x 10^{-6} mbar using a turbo-molecular pump backed by a two stage, oil sealed, rotary vane pump. After being evacuated at this pressure for two hours the vacuum chamber was isolated from the pumping system by means of a gate valve and backfilled to 500 mbar with N_2 gas. Samples were heated, in fused quartz crucibles, by induction heating of a graphite susceptor contained within an alumina shell. Viewing slots were cut into the susceptor and alumina to allow the sample to be viewed through a window in the chamber. Melt encasement, within a high purity flux, was employed to reduce the number of potential heterogeneous nucleation sites allowing the attainment of high undercoolings. Normally, for a material with a melting point > 1300 K a soda-lime glass flux would be used, however, due to a reaction between the soda-lime and the metal a B_2O_3 flux was used instead. Prior to performing the undercooling experiments the B_2O_3 flux was dehydrated for one hour by heating to just below its melting point under high vacuum.

Temperature determination was by means of an R-type thermocouple positioned beneath the crucible, which had been thinned at the base so reducing the thermal lag between the sample and thermocouple. Cooling curves were obtained with the aid of a chart recorder. A schematic diagram of the experimental apparatus is shown in Figure 2. By heating the sample to its melting temperature, cooling and repeating this procedure, it was found that melting temperatures were reproducible to within $\pm$ 5 K.

During a typical undercooling experiment the alloy would be superheated to 200 K above its melting point and, in order to achieve the highest undercoolings reported here, several heating-cooling cycles would be performed. Once the desired undercooling was obtained solidification was nucleated by touching the sample surface with a thin trigger needle that was pushed through the flux. The experimental method is described in more detail in [23, 24].

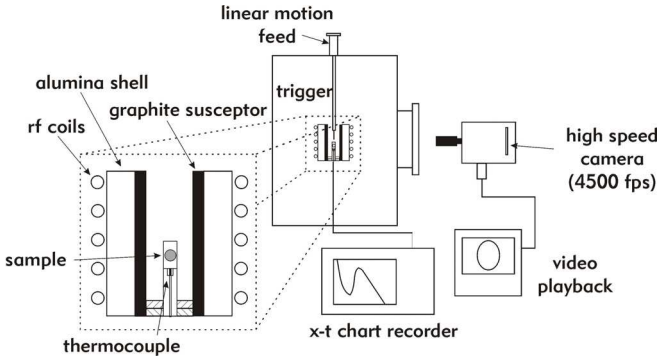

Figure 2. Schematic diagram of the melt fluxing apparatus used to undercool Ni-Si.

High speed photography is a well established technique for determining the recalescence velocity during the solidification of deeply undercooled metallic melts [25]. Here, solidification velocities were determined by filming the progress of the recalescence front across the droplet at high frame rate (4500 fps) using a Kodak Ektapro 4050mx high speed motion analyser. The position of the front was identified in a number of frames representing the interval from nucleation to completion of solidification. Computer simulation of the progress of the front was used to determine the position of the nucleation point, which could subsequently be checked against the as-solidified sample, and the velocity of progegation of the front. In the simulation the solidification front is assumed to grow spherically outwards from the nucleation point at uniform velocity. The 2-dimensional projection of the intersection of the solidification front with the surface of the droplet is calculated and a series of simulated images constructed which may be compared with those obtained by high speed photography. By determining the best match to the experimental data the actual velocity of the solidification front can be reconstructed.

3. Results

A maximum undercooling of $\Delta T = 160$ K was attained for this material by using cyclic fluxing and superheating, as described in the Experimental Methods section above. Unusually for a deeply undercooled melt, considerable difficulty was encountered in nucleating solidification with a trigger needle. The material was almost completely impervious to triggering with the alumina needle normally used with our fluxing system, to the extent that the needle could be inserted into the sample and rotated, thus stirring the undercooled melt without initiating solidification. The nucleation potency of the needle was subsequently improved by adding an Ni-Al tip to the trigger needle, although even with this modification solidification could not be triggered below an undercooling of 60 K. We also note that upon attempting to withdraw the trigger needle from an undercooled droplet in which contact with the needle had not initiated nucleation, the melt appeared to be unusually viscous and that

it was possible to pull the droplet into a 'teardrop' shape. We have previously used the melt fluxing technique reported here to study a range of other deeply undercooled pure materials (Ge [23], Cu [24]) and alloys (Cu-Sn [26], Ge-Fe [27], Ni-Ge [21], Ag-Cu, Co-Sn) and have not observed this type of behaviour in any other system. Moreover, as described in Section 2 above, for relatively high melting point materials such as Ni-Si we would normally use a soda-lime glass flux, although that was not possible in this case due to a reaction between soda-lime and the metal. Consequently, B_2O_3 flux was used instead, despite this flux displaying a very low viscosity at the melting point of the Ni-25.2 at.% Si alloy. We therefore conclude that the viscosity effects observed during the undercooling experiments on Ni-25.2 at.% Si are anomalous, even for an undercooled melt and are characteristic of the metal, not the flux or the technique used. However, no facility was available to measure the viscosity of the undercooled melt whilst encased in a glass flux, so although we believe the undercooled melt to be of high viscosity this cannot be quantified.

Upon triggering, all samples displayed double recalescence. By using high frame rate video recording, a limited number of growth velocity measurements were obtained for the first of these recalescence events, with these measurements corresponding to samples at the higher end of the undercooling range achieved ($125\ \text{K} \leq \Delta T \leq 160\ \text{K}$). These results are summarised in Fig. 3. All data points correspond to solidification events that have been initiated via touching the sample with a trigger needle and in which a single recalescence front can be observed to progress smoothly across the sample. From the figure it is clear that the observed growth velocities, peaking at $0.018\ \text{m s}^{-1}$ (for an undercooling of $\Delta T = 160\ \text{K}$), are exceptionally low, even when compared with those reported in other intermetallic systems [18, 20, 21]. Below $\Delta T \leq 125\ \text{K}$ growth was so sluggish that the velocity could not be determined accurately ($V \leq 0.005\ \text{m s}^{-1}$). In a limited number of cases filming of the second recalescence event was possible, from which it was apparent that recalescence started from random, and in some cases multiple, sites within the sample. Consequently, it was not possible to obtain meaningful data relating to the rate of progress of the second recalescence event.

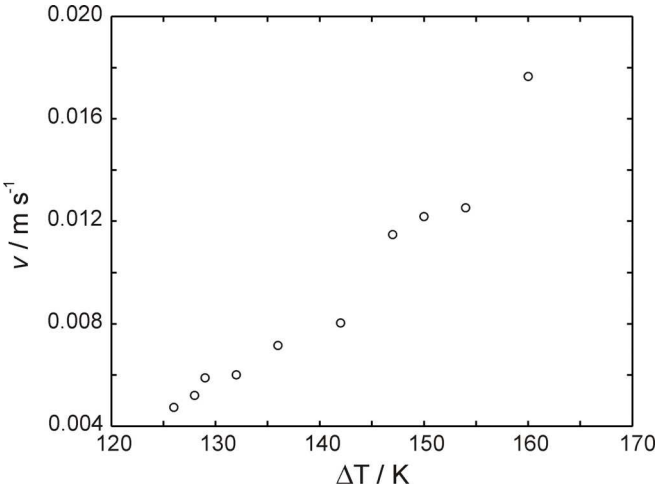

Figure 3. Velocity-undercooling curve for the solidification of Ni-25.2 at.% Si.

There is no clear indication from Fig. 3 of distinct growth regimes and consequently samples spanning a range of undercoolings have been selected for microstructural analysis. An SEM micrograph taken from a sample undercooled by 80 K prior to nucleation is shown in Fig. 4. This corresponds to the region of the phase diagram in which direct access to the β_3 phase should be possible. Secondary (backscatter) electron detection has been used to provide atomic number contrast, which will effectively map the silicon content within the sample. The observed structure is very clearly eutectic, consisting of alternating regions of high and low silicon content with a typical lamella spacing of the order of 15-20 μm. Moreover, some additional, very fine structure is evident in the Ni-rich lamellae. This is shown in more detail in a high resolution FEGSEM image (Fig. 5).

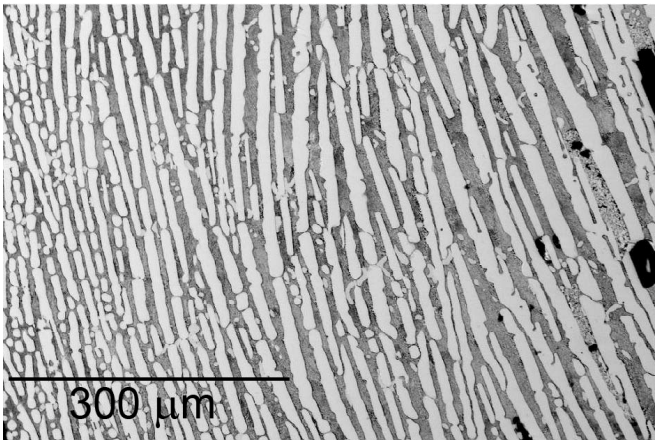

Figure 4. SEM micrograph (backscatter detection) showing the microstructure of a sample undercooled by 80 K prior to nucleation of solidification. The structure consists of alternating lamellae of Ni- and Si-rich phases.

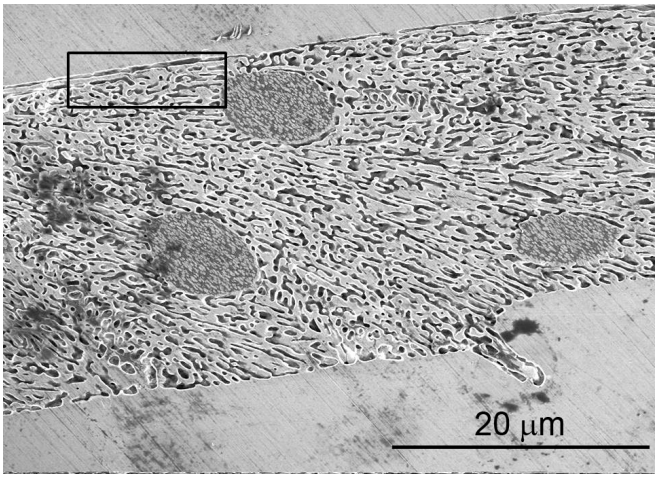

Figure 5. High resolution FEGSEM micrograph showing extensive internal structure within the Ni-rich lamellae for the sample undercooled by 80 K prior to nucleation of solidification (rectangular box indicates area selected for TEM analysis).

The Si-rich lamellae appear to be single phase but a very complex morphology is evident in the Ni-rich lamellae. In order to identify the phases present in the Ni-rich lamellae a TEM micrograph (Fig. 6) has been obtained for a small region of the sample, the location of which is shown by the box in Fig. 5. From figures 5 and 6 it is clear that the coarse, Si-rich lamellae consist of single phase γ ($Ni_{31}Si_{12}$), while the Ni-rich lamellae consist predominantly of a continuous matrix of βNi_3Si in which are discontinuous inclusions or lamellae of αNi, which are typically 200-400 nm thick. However, within the Ni-rich lamellae there are also nodular features, typically < 10 μm in diameter, wherein this structure is inverted and in which it is the αNi that is the continuous phase. These nodules also appear to be more Ni-rich than the rest of the lamellae and to have a finer distribution of αNi and βNi_3Si than is the case in the rest of the lamellae. From the phase diagram any γ present would be expected to react peritectically to give βNi_3Si. The characteristic peritectic morphology would be for a shell of βNi_3Si to surround a core of unreacted γ, although no such features are evident here.

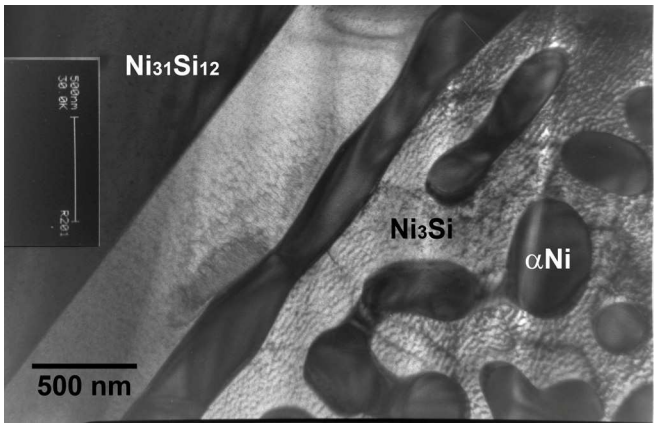

Figure 6. TEM micrograph of the boundary between the Ni- and Si-rich lamellae in the sample undercooled by 80 K prior to nucleation of solidification. The Si-rich regions are single phase γ ($Ni_{31}Si_{12}$), while the Ni-rich lamellae consist of isolated regions of αNi in a matrix of βNi_3Si.

To ensure that the structure determined by high resolution FEGSEM and TEM analysis is representative over a larger area of the material, EBSD phase mapping has also been undertaken, the results of which are shown in Fig. 7. Although it is clear that the EBSD micrograph has insufficient resolution to adequately resolve the detail of the very fine structures observed in the Ni-rich lamellae that were apparent using TEM, the broad picture is consistent, with single phase lamellae of γ interspersed with lamellae containing an exceptionally fine distribution of αNi and βNi_3Si. Moreover, the β-phase appears to be almost exclusively in the low temperature β_1 form.

Little change in the morphology is observed as the undercooling is increased. FEGSEM and EBSD micrographs are shown in Figures 8 and 9 respectively, for a sample undercooled by 132 K prior to nucleation. This undercooling is in the region in which solidification to the (ordered) β_2Ni_3Si polymorph might be expected. However, the structure is broadly similar to that observed at temperatures corresponding to the (disordered) β_3Ni_3Si stability field, being still largely eutectic in character. However, the Si-rich regions of single phase γ now appear to have

undergone fragmentation into discrete plate like structures. This may be the result of a remelting of the eutectic lamellae during recalescence, with post-recalescence remelting of γ having also been reported by [11]. The Ni-rich regions still predominantly consist of a fine dispersion of αNi and β_1Ni_3Si, although there are now regions containing significant amounts of β_3Ni_3Si. This is relatively coarse in nature suggesting that, like the γ-phase, it grew during the primary recalescence event. This is not the equilibrium polymorph for the temperature at which growth was initiated and may therefore indicate that some disorder trapping may have taken place. There also appear to be small amounts of the metastable $Ni_{25}Si_9$ randomly interspersed across the structure.

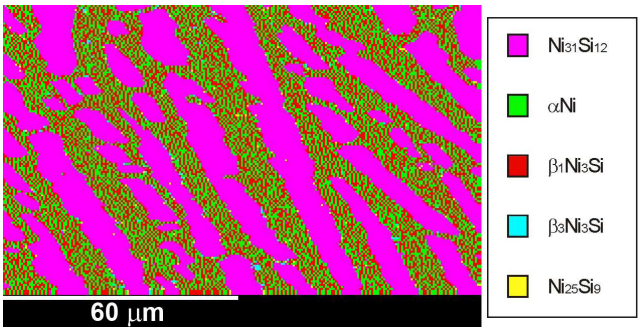

Figure 7. EBSD phase analysis of the sample undercooled by 80 K prior to nucleation of solidification, showing that the structure of single phase γ lamellae alternating with Ni-rich lamellae of finely dispersed αNi and βNi_3Si is representative of large areas of the specimen.

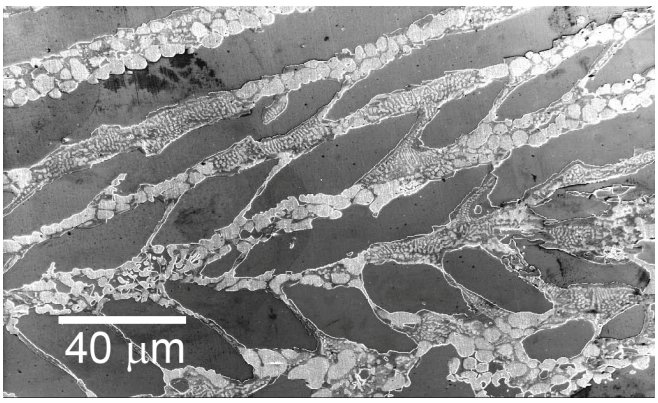

Figure 8. High resolution FEGSEM micrograph of a sample undercooled by 132 K prior to nucleation of solidification. Alternating lamellae of single phase γ and finely dispersed α/β are still evident but fragmentation of the γ-phase appears to have occurred, possibly via a Rayleigh instability mechanism.

As a further check that the eutectic structures described above are characteristic of the whole sample, a photo-montage of the droplet undercooled by 132 K is shown in Fig. 10. With the exception of a region around the area where the trigger needle was inserted into the sample (top left corner of image), the eutectic structure is highly regular, with the lamellae oriented approximately parallel to the growth direction, which for this sample was from the top left of the sample towards the bottom right.

Significant damage to the sample is evident where the trigger needle was inserted, and indeed it appears that the needle penetrated some 440 μm into the sample. This is highly unusual as in most metals undercooled to this level solidification would be initiated almost immediately upon contact with the trigger and virtually no penetration into the sample would be expected. Again this would seem to indicate a material that is resistant to nucleation. We have previously observed evidence [28, 29] of flow induced deformation in materials processed via the flux encasement technique when electromagnetic heating is used to melt the sample, as it is here. However, the highly regular structure observed in the eutectic would suggest that this is not the case here, which may be related to the apparent high viscosity of the melt.

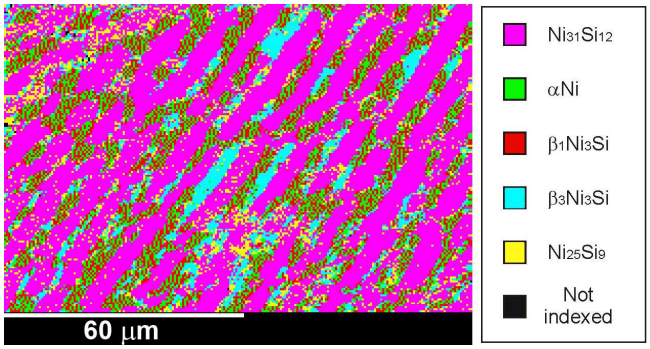

Figure 9. EBSD phase analysis of the sample undercooled by 132 K prior to nucleation of solidification. As at lower undercooling the structure is still predominantly of alternating lamellae of γ and finely dispersed α/β, although some fragmentation of the γ is apparent. Some of the Ni-rich regions now appear to contain the high temperature β_3 form of Ni_3Si. Small amounts of metastable $Ni_{25}Si_9$ are also evident dispersed across the sample.

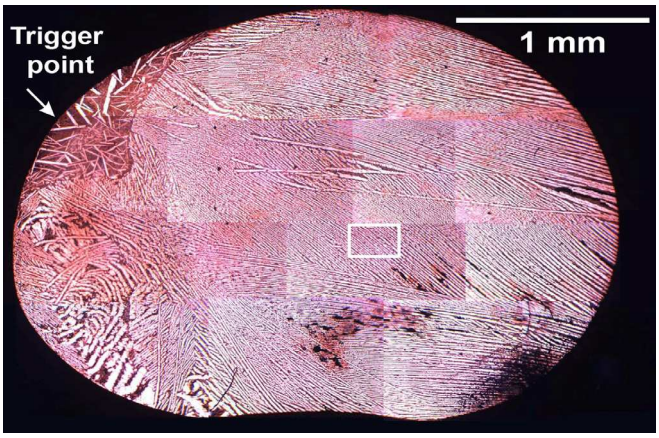

Figure 10. Montage of optical micrographs across the sample undercooled by 132 K prior to solidification, showing highly regular eutectic like structure across the entire sample. Note the region of extensive damage in the top left of the sample where the trigger needle was inserted. The estimated penetration depth into the sample is 440 μm. The region from which the samples for FEGSEM and EBSD analysis were taken is shown by the box.

4. Discussion

The primary solidification morphology for Ni-25.2 at.% Si appears to be a lamellar eutectic structure, in which there is an Si-rich phase, which is pure γ ($Ni_{31}Si_{12}$) and an Ni-rich phase. Eutectic growth would be consistent with the very low growth velocities observed for the primary recalescence event, which even for undercoolings of $\Delta T = 160$ K, do not exceed 0.018 m s^{-1}. Indeed, the low solidification velocities observed here appear to be consistent with a general trend that may be observed by comparing previous studies on the Ni-rich end of the Ni-Si phase diagram: namely that the solidification velocity drops with increasing Si concentration. Leonhardt *et al*. [5] measured a maximum growth velocity of 1.5 m s^{-1} for the Ni-21.4 at.% Si eutectic alloy (based on an undercooling of 220 K), but much high velocities of up to 7 m s^{-1} in the hypoeutectic alloy. Yet higher velocities were measured by Cochrane *et al*. [30]. For Ni-Si alloys with Si content of 11.8 at.% Si they observed growth velocities of 24 m s^{-1} ($\Delta T \approx 260$ K) while at 2.07 at.% Si velocities approaching 60 m s^{-1} were observed at similar undercoolings.

The Ni-rich phase in the eutectic structure formed from solidifying undercooled Ni-25.2 at.% Si alloy appears to subsequently undergo a further decomposition, probably via a solid-state reaction, to give an extremely fine (200-400 nm) eutectoid structure consisting of αNi and βNi_3Si. This would be consistent with the observation of a second recalescence event, which has previously been associated with a solid-state transition occurring shortly after primary solidification [25]. Unfortunately, we have not been able to make any growth velocity measurements for this reaction as, in the limited number of instances in which the transition was filmed, multiple nucleation events were evident. In one case, corresponding to a sample with an undercooling for primary solidification of 87 K, we were able to determine the temperature at which the second recalescence event occurred, this being ~1200 K, some 63 K below the lower temperature limit at which the high temperature β_2 phase would be expected to be stable.

However, this solidification pathway, even with significant departures from equilibrium, does not appear to be consistent with the phase diagram. In order to analyse the solidification morphology further CALPHAD modelling has been undertaken, as above using the software package MTDATA [16]. We postulate that direct solidification of β from the liquid is suppressed at this composition, possibly as a result of nucleation of the β-phase being inhibited. Under these assumptions the equilibrium morphology in this region of the phase diagram would be a eutectic between γ and αNi. In fact, suppressing growth of the β-phase has only a minor effect on the location of the eutectic point, with the α-γ eutectic occurring at a temperature approximately 14.5 K lower and at a concentration which is 0.6 at.% more Si-rich than the α-β eutectic (i.e. the eutectic composition would be Ni-22.0 at.% Si, so that Ni-25.2 at.% Si would be hypereutectic).

Similar behaviour has been observed in Nb- xSi (x = 21.0 - 27.0 at.%) alloys, where for undercoolings in excess of 270 K (based on the equilibrium phase-diagram) direct solidification to primary Nb_3Si should be observed. However, Bertero *et al*. [31] found that in levitated drops of these alloys, primary solidification was to a metastable α-Nb + β-Nb_5Si_3 eutectic, an observation they attributed to difficulty in nucleating the Nb_3Si phase. Such behaviour would be consistent with the solidification

morphologies observed here and with the fact that the undercooled melt was extremely resistant to triggering, to an extent that we have not witnessed before in any melts at this level of undercooling.

From the EBSD analysis (Fig. 7) it is possible to estimate the volume fractions of the various phases. For the sample undercooled by 80 K prior to nucleation around 48% of the sample comprises γ. Based on the initial Si concentration of the alloy (25.2 at.% Si) and a concentration for γ based on its stoichiometry ($Ni_{31}Si_{12}$ = 27.9 at.% Si) it is possible to estimate the Si concentration of the Ni-rich lamellae, which is around 22.3 at.% Si. This compares with a maximum equilibrium solubility for Si in αNi of around 16 at.% Si. Consequently, if we assume that initial solidification event, corresponding to the first recalescence event, is the growth of an α-γ eutectic with around 48 % γ, considerable extended solubility of Si in the αNi phase would also need to be invoked. The resulting supersaturated α is likely to be highly metastable, and the subsequent eutectoid decomposition to β-Ni_3Si and a less supersaturated α-phase would not be surprising.

However, the results presented here raise two fundamental questions regarding this material (i) why is the direct solidification of β from the liquid, a phase that is observed to grow easily at the eutectic composition, suppressed in this case and (ii) given that the growth velocities observed are so low, why is such a large extended solid solubility observed for Si in α-Ni? In this regard we note the anomalously high viscosity of the undercooled melt remarked upon in the results sections and believe that this may be a key observation to understanding these results. Such a high viscosity might arise if there were a tendency for the formation of Si networks within the melt or due to unusually high levels of short range order or clustering in the liquid. The formation of such structures has been observed by neutron diffraction in the alloys NiSi and $NiSi_2$ by Gruner *et al*. [32], who comment that the structure of the Ni-Si liquid is strongly influenced by the tendency of Si atoms to form covalent bonds and moreover that in the case of the $NiSi_2$ alloy the structure of the liquid resembles that of the ordered solid alloy.

A high viscosity in the undercooled melt would imply that its diffusion coefficient would be unusually low. This would lead to low growth velocity for the solid and may inhibit the nucleation of certain phases, as the time required for the formation of a critical cluster size would become long due to low atomic mobility, particularly for crystal structures with a complex unit cell, or in which the structure of the solid were significantly different from any structure that may exist in the liquid. Moreover, it may lead to solidification morphologies in which diffusion of solute over short distance, such as eutectics, is favoured over morphologies in which longer range diffusion is required, such as the formation of single-phase dendrites, even if the eutectic is not the thermodynamically most stable phase. A low diffusion coefficient might also result in significantly extened solid solubility, as appears to occur here in the αNi phase. Such a model would appear to fit the observational evidence presented here, and may also account for the observation of Lu *et al*. [13] that some binary Ni-Si alloys may display small fractions of amorphous phase formation at unusually low cooling rates if solidified from deeply undercooled melts.

5. References

1. P.H. Thornton & R.G. Davies, Temperature dependence of flow stress of gamma prime phases having L_{12}, structure, Metall. Trans. 1 (1970) 549.
2. S. Milenkovic, R. Caram, Effect of the growth parameters on the Ni-Ni_3Si eutectic microstructure, J. Cryst. Growth 237 (2002) 95-100.
3. R.W. Cahn, P.A. Siemers, J.E. Geiger, P. Bardham, The order-disorder transformation in Ni3Al and Ni3Al-Fe alloys: 1. Determination of the transition-temperatures and their relation to ductility, Acta Metall. 35 (1987) 2737-2751.
4. B. Wei, D.M. Herlach, Rapid solidification of bulk undercooled Ni-21.4 at %Si eutectic alloy, Trans. Mat. Res. Soc. Jpn. 14A (1995) 639 - 642.
5. M. Leonhardt, W. Loser, H.G. Lindenkreuz, Metastable phase formation in undercooled eutectic $Ni_{78.6}Si_{21.4}$ melts , Mater. Sci. Eng. A271 (1999) 31-37.
6. Y.P Lu, F. Liu, G.C Yang, H.P. Wang, Y.H. Zhou, Grain refinement in solidification of highly undercooled eutectic Ni-Si alloy, Mater. Lett. 61 (2007) 987-990.
7. F. Liu, Y.Z. Chen, G.C Yang, Y.P Lu, Z. Chen, Y.H. Zhou, Competitions incorporated in rapid solidification of the bulk undercooled eutectic $Ni_{78.6}Si_{21.4}$ alloy, J. Mater. Res. 22 (2007) 2953-2963.
8. M. Schwarz, A. Karma, K. Eckler, D. M. Herlach, Physical-mechanism of grain-refinement in solidification of undercooled melts, Phys. Rev. Lett. 73 (1994) 1380-1383.
9. A.M. Mullis, R.F. Cochrane, Grain refinement and the stability of dendrites growing into undercooled pure metals and alloys, J. Appl. Phys. 82 (1997) 3783-3790.
10. A. M. Mullis, R. F. Cochrane, A phase field model for spontaneous grain refinement in deeply undercooled metallic melts, Acta Mater. 49 (2001) 2205-2214.
11. Y.P Lu, F. Liu, G.C Yang, Y.H. Zhou, Composite growth in highly undercooled $Ni_{70.2}$ $Si_{29.8}$ eutectic alloy, App. Phys. Lett. 89 (2006) 241902.
12. Y.P Lu, X. Lin, G.C Yang, J. Li, Y.H. Zhou, The formation of quasiregular microstructure in highly undercooled Ni(70.2)Si(29.8) eutectic alloy, J. Appl. Phys. 104 (2008) 013535.
13. Y.P Lu, G.C Yang, J. Li, Y.H. Zhou, Amorphous Formation in an Undercooled Binary Ni-Si Alloy under Slow Cooling Rate, J. Mater. Sci. technol. 25 (2009) 370-372.
14. R.W. Cahn, P.A. Siemers, J.E. Geiger, P. Bardham, The order-disorder transformation in Ni3Al and Ni3Al-Fe alloys: 1. Determination of the transition-temperatures and their relation to ductility, Acta Metall. 35 (1987) 2737-2751.
15. T.B Massalski, P.R. Subramanian, H. Okamoto, L. Kacprzak. 'Binary Alloy Phase Diagrams, 2nd ed.' ASM International, Materials Park,OH, 1990.
16. MTDATA is licensed by the National Physical Laboratory, UK.
17. The CALPHAD calculations reported here were conducted using version 5 of the SGTE solutions database (Dec. 2010). See www.sgte.org.
18. D.M. Herlach, Metastable materials solidified from undercooled melts, J. Phys. Condens. Mater. 13 (2001) 7737-7751.
19. C.D. Anderson, W.H. Hofmeister, R.J. Bayuzick, Solidification kinetics and metastable phase formation in binary Ti-Al, Metall. Trans. A 23 (1992) 2699-2714.

20. G. Phanikumar, K. Biswas, O. Funke, D. Holland-Moritz, D.M. Herlach, K. Chattopadhyay, Solidification of undercooled peritectic Fe-Ge alloy, Acta Mater. 53 (2005) 3591-3600.
21. R. Ahmad, R.F. Cochrane, A.M. Mullis, Disorder trapping during the solidification of βNi_3Ge from its deeply undercooled melt, J. Mater. Sci., in press.
22. H. Assadi, A.L. Greer, Modelling of kinetics of solidification of intermetallic compounds, Mat. Sci. Eng. A 226 (1997) 70-74.
23. S.E. Battersby, R.F. Cochrane, A.M. Mullis, Highly undercooled germanium: Growth velocity measurements and microstructural analysis, Mater. Sci. Eng. A 226 (1997) 443-447.
24. K. Dragnevski, R.F. Cochrane, A.M. Mullis, Experimental Evidence for Dendrite Tip Splitting in Deeply Undercooled, Ultra-High Purity Cu, Phys. Rev. Lett. 89 (2002) 215502.
25. B.T. Bassler, W.H. Hofmeister, R.J. Bayuzick, R. Gorenflo, T. Bergman, L. Stockum, Observation of alloy solidigfication using high-speed video, Rev. Sci. Instrum. 63 (1992) 3466-3470.
26. S.E. Battersby, R.F. Cochrane, A.M. Mullis, Microstructural evolution and growth velocity-undercooling relationships in the systems Cu, Cu-O and Cu- Sn at high undercooling, J. Mater. Sci. 35 (2000) 1365-1373.
27. S.E. Battersby, R.F. Cochrane, A.M. Mullis, Growth velocity-undercooling relationships and microstructural evolution in undercooled Ge and dilute Ge-Fe alloys, J. Mater. Sci. 34 (1999) 2049-2056.
28. K. Dragnevski, A.M Mullis, D.J. Walker, R.F. Cochrane, Mechanical deformation of dendrites by fluid flow during rapid solidification, Acta Mater. 50 (2002) 3743-3755.
29. A.M Mullis, D.J. Walker, S.E. Battersby, R.F. Cochrane, Deformation of dendrites by fluid flow during rapid solidification, Mater. Sci. Eng. A 304-306 (2001) 245-249.
30. R.F. Cochrane, A.L. Greer, K. Eckler & D.M. Herlach, Dendrite growth velocities in undercooled Ni-Si alloys, Mat. Sci. Eng. A. 133 (1991) 698-701.
31. G.A. Bertero, W.H. Hofmeister, M.B. Robinson, R.J. Bayuzick, Containerless processing and rapid solidification of Nb-Si alloys of hypereutectic composition, Metall. Trans. A 22 (1991) 2723-2732.
32. S. Gruner, J. Marczinke, L. Hennet, W. Hoyer, G.J. Cuello, On the atomic structure of liquid Ni-Si alloys: a neutron diffraction study, J. Phys.: Condens. Mat. 21 (2009) 385403.